ISIJ International, Vol. 52 (2012), No. 6, pp. 1153–1161

A Modeling Approach to Evaluate Grain Interaction Induced by {111}<01$\bar{1}$> Planar Slips in Face-centered Cubic Polycrystalline Materials

Motoaki MORITA[1)] and Osamu UMEZAWA[2)]

1) Graduate School of Engineering, Yokohama National University, 79-5 Tokiwadai, Hodogaya-ku, Yokohama, Kanagawa, 240-8501 Japan. E-mail: morita-motoaki-pm@ynu.jp 2) Faculty of Engineering, Yokohama National University, 79-5 Tokiwadai, Hodogaya-ku, Yokohama, Kanagawa, 240-8501 Japan.

(*Received on January 13, 2012; accepted on January 23, 2012*)

An accommodation deformation model to relax incompatibility between soft (yielded) and hard (non-yielded) grains was proposed. Dislocation arrays were installed in the soft grain to investigate the effect of secondary slips on accommodating the displacement incompatibility due to the grain interaction at the grain boundary. When a secondary slip in the soft grain is active on the same plane as the dislocation arrays, it can accommodate the displacement incompatibility in almost all orientations. However, a dislocation reflection on the primary slip plane is difficult to adopt for accommodation deformation. When the secondary slip in the soft grain is restricted to a plane without the primary slip, accommodation deformation in the soft grain does not occur. To accommodate the displacement incompatibility at the grain boundary, slip systems in the adjacent grain are required in almost all orientations. Around the orientation at which the secondary plastic deformation is the hardest to achieve, three slip systems are operating in areas of accumulation with high displacement incompatibility. Thus, the three slip systems should operate on different octahedral slip planes. However, the displacement incompatibility is not fully accommodated, and a stress field remains near the normal to {111}. The combination of sufficient stress concentration to open the grain boundary and the assembly of dislocations on the three slip systems at the grain boundary may be the cause of intergranular cracking.

KEY WORDS: subsurface crack initiation; Taylor theory; austenitic steel; high-cycle fatigue; stress concentration; heterogeneous deformation; incompatibility.

1. Introduction

It is generally understood that fatigue crack initiation on a specimen surface occurs via slip deformation due to an irreversible process of extrusion and intrusion. However, subsurface crack generation in high-cycle fatigue has been reported for titanium alloys[1–10)] and nitrogen-strengthened austenitic steels[11–14)] and typically occurs at low temperature. The crack initiation sites in the materials are highly crystallographic transgranular or intergranular cracks called facets. For transgranular cracking in α-titanium alloys,[1–10)] a fractographic fracture of the microcrack and its growth is evident. In the case of intergranular cracking, mismatched line traces on the matching facets of opposing fracture surfaces appeared in nitrogen-strengthened austenitic steel.[11)] Crystallographic pits and protrusions were also detected on the intergranular facets and were interlocked on opposite sides, and thus the opening stress, which is normal stress at the grain boundary, must be involved. However, fractographic analyses alone cannot elucidate the microcracking mechanism.

Subsurface fatigue crack generation was typically detected when the maximum applied stress level is lower than the yield strength (0.2% proof stress) under uniaxial loadings.[12)] Thus, a dislocation arrangement as pile-ups was developed only in the soft grains because of the locally yielded materials. Dislocation arrays of a restricted slip system, which are commonly observed in cyclically deformed materials, are blocked at the grain boundaries resulting in a concentration of stress. Electron back-scattered diffraction (EBSD) analysis provides further evidence of local stress concentration due to the grain interaction (incompatibility) at the grain boundaries.[13)] Although it has been commonly noted that a local stress concentration results in transgranular cracking or intergranular cracking to reduce the stress,[4–13)] the cracking mechanisms have yet to be clarified. Stroh[15)] proposed a cleavage fracture model for titanium alloys that involves a number of dislocations accumulated at a grain boundary, which produces a microcrack. A slip-off on {111} in nitrogen-strengthened austenitic steel has also been discussed as a cause of transgranular cracking.[16–18)] These models suggest that piled-up dislocations form a microcrack. Based on the fractographic features and microcracking models mentioned above, it is believed that normal stress at the grain boundary in combination with a number of dislocations causes intergranular cracking. However, there is no

direct evidence to support the involvement of interactions between localized planar slips and microcracks in the interior of the specimen. Thus, an analytical approach is necessary to discuss the relationship between localized arrays and grain interactions at the grain boundary. In the present study, we adopted an advanced relaxed-constraints (RC) model to predict the operation of localized planar slips and their accommodation at the grain boundaries due to grain interactions.

Classical Taylor full-constraints (FC) model[19] assumes full strain continuity and neglects the stress equilibrium at the grain boundary. Namely, the local velocity gradient, l_{ij}, in a grain is equal to the macro velocity gradient, L_{ij}, and thus the operation of five independent slip systems is required. On the other hand, the RC model[20] allows local incompatibility between adjacent grains; it can include the relaxation of components of the local velocity gradient, l_{pq} (p, q: any of i, j) at the boundary. Thus, l_{pq} is equal to a free variable.[20] Consequently, the relaxation of l_{pq} results in a reduction of the number of slip systems operated, and causes plastic work (deformation energy) to be between the upper (strain homogeneity in the FC model) and lower bounds (stress homogeneity in the Sachs model[21]). In the RC model, the compatibility of l_{pq} is not maintained, whereas the compatibility of σ_{pq} is guaranteed at the grain boundary. Here, a flat and infinite grain interface between grains A and B is taken with the coordination (interface normal, x_1) shown in **Fig. 1**. The following equations must be satisfied for a static equilibrium of stress:

$$\sigma_{11}^{A} = \sigma_{11}^{B},\ \sigma_{12}^{A} = \sigma_{12}^{B},\ \sigma_{13}^{A} = \sigma_{13}^{B}, \quad \text{..... (1)}$$

Equation (1) can be satisfied when l_{11}, l_{12}, and l_{13} are relaxed under an assumption of heterogeneous deformation near the grain boundary. The basic approach in the RC model is the relaxation of displacement compatibility in favor of improved stress homogeneity between adjacent grains. However, a heterogeneous deformation near the grain boundary is actually ignored during the analysis. To satisfy both the continuities of stress and displacement, the advanced RC model[20,22–26] takes the grain interaction into account, in which σ_{pq} can be specified beforehand and is generally assumed to be zero. When l_{pq} is relaxed in a grain, the relaxation causes a misfit of the velocity gradient, δ_{pq}, between it and a neighboring grain. The value of δ_{pq} is generally given by the elastic deformation and/or geometrically necessary dislocations (GNDs). In the case of a saturated dislocation structure under a cyclic deformation, a concentration of stress at the boundary causes an emission of dislocations in the adjacent grain.[11] The emitted dislocations may result in GNDs. Here, we consider σ_{pq}, which can induce a secondary slip deformation such as an emission. Thus, l_{pq} and σ_{pq} give the opening displacement and opening stress at the grain boundary, respectively. To understand the intergranular cracking that occurs under high-cycle fatigue in nitrogen-strengthened austenitic steel, in the present study, we evaluated slip deformation from grain interaction at a grain boundary using the advanced RC model, as models based on the Taylor theory can be used to easily install the constraints condition and analyze the dependence of a deformation on the crystal orientation. Therefore, the active slip systems and their slip rates in both a grain and the grain adjacent to it were evaluated to determine the mechanism for the accommodation of displacement incompatibility due to grain interaction at the grain boundary when the dislocation arrays are operated by $\{111\}<01\bar{1}>$ systems in a soft grain.

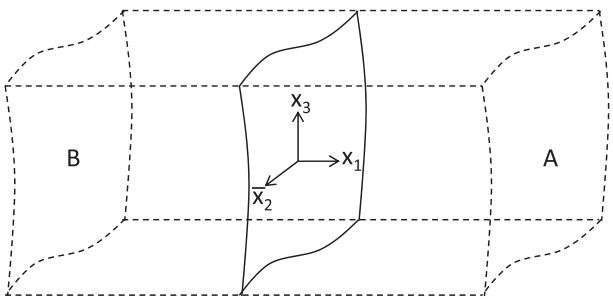

Fig. 1. Force equilibrium at grain boundary.

2. Procedure

2.1. Slip Deformation Based on Taylor Theory

Models based on the Taylor theory usually neglect elastic strain. The velocity gradient, l_{ij}, describes a local deformation using the slip rates of all active slip systems:

$$l_{ij} = \Omega_{ij} + \sum_{k} b_i^{(k)} n_j^{(k)} \dot{\gamma}^{(k)}, \quad \text{..... (2)}$$

where $b^{(k)}$ is the unit vector in the slip direction of slip system k, $n^{(k)}$, is the unit vector normal to the slip plane of slip system k, and $\dot{\gamma}^{(k)}$ is the slip rate of slip system k. The velocity gradient, *i.e.*, $l_{ij} = b_i^{(k)} n_j^{(k)} \dot{\gamma}^{(k)}$, includes the plastic strain rate, D_{ij}^{P}, and the plastic spin, W_{ij}^{P}, as follows:

$$l_{ij} = \Omega_{ij} + D_{ij}^{P} + W_{ij}^{P}, \quad \text{..... (3)}$$

$$D_{ij}^{P} = \frac{1}{2}(b_i^{(k)} n_j^{(k)} \dot{\gamma}^{(k)} + b_j^{(k)} n_i^{(k)} \dot{\gamma}^{(k)}), \text{ and} \quad \text{..... (4)}$$

$$W_{ij}^{P} = \frac{1}{2}(b_i^{(k)} n_j^{(k)} \dot{\gamma}^{(k)} - b_j^{(k)} n_i^{(k)} \dot{\gamma}^{(k)}), \quad \text{..... (5)}$$

where the lattice spin, Ω_{ij}, depends on the constraints condition and accommodates the incompatibility due to W_{ij}^{P}. In the present study, it is assumed that Ω_{ij} is zero, and the incompatibility induces a secondary plastic deformation.

2.2. Accommodation Deformation Model

To evaluate the incompatibility normal to the grain boundary plane, two adjacent grains, soft grain (yielded) A, and hard grain (non-yielded) B, are put into the tension mode along the x_3 axis, as shown in **Fig. 2**. In addition, the displacements along all axes at points 1 and 5 are constrained, as are the displacements along the x_2 and x_3 axes at points 2, 3, 4, and 6. The velocity gradients, l_{11}, l_{12}, and l_{13}, give the opening displacements when the tensile direction is parallel to the x_3 axis (**Fig. 3**). Here, the corner of the grain boundary is not responsible for the interactions between the grains. The following equation satisfies the compatibility of the displacement normal to the grain boundary:

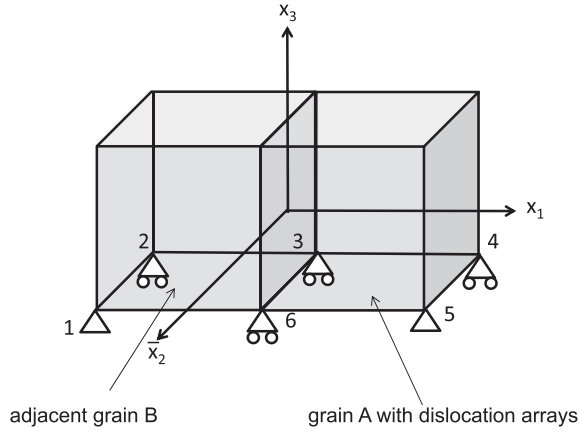

Fig. 2. Schematic arrangement of two grains under accommodation deformation.

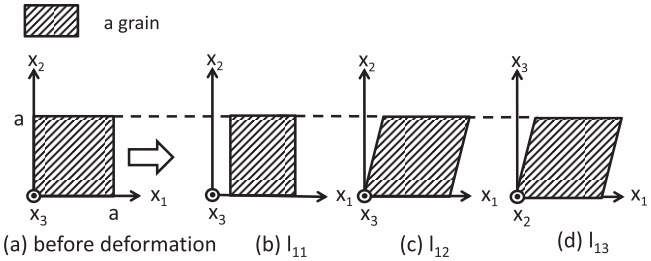

Fig. 3. Schematic illustration of the velocity gradient.

$$l_{11}^{A} = -l_{11}^{B},\ l_{12}^{A} = l_{12}^{B},\ l_{13}^{A} = l_{13}^{B} \quad \text{..... (6)}$$

Dislocation arrays installed only in grain A generate the grain interaction between grains A and B. To accommodate the displacement incompatibility due to the grain interaction at the grain boundary, a secondary plastic deformation should be induced in either grain A or B. The secondary deformation is independent of its slip length. The velocity gradient, l_{ij}, causes a velocity gradient misfit, δ_{ij}, between the grains according to the following equation:

$$\delta_{11} = l_{11}^{A}, \delta_{12} = l_{12}^{A}, \delta_{13} = l_{13}^{A}. \quad \text{..... (7)}$$

When the secondary plastic deformation in grain A relaxes the velocity gradient misfit, the velocity gradient, $l_{ij}^{acc(A)}$, becomes equivalent to $-\delta_{ij}$.

$$l_{11}^{acc(A)} = -\delta_{11}, l_{12}^{acc(A)} = -\delta_{12}, l_{13}^{acc(A)} = -\delta_{13} \quad \text{..... (8)}$$

Plastic deformation in the adjacent grain, B, can also relax the misfit. The velocity gradient $l_{ij}^{acc(B)}$ is expressed as

$$l_{11}^{acc(B)} = -\delta_{11}, l_{12}^{acc(B)} = \delta_{12}, l_{13}^{acc(B)} = \delta_{13} \quad \text{..... (9)}$$

It is assumed that the slip rate of the arrays, $\dot{\gamma}^{arrays}$, in grain A is constant as the dislocation structure is saturated. $\dot{\gamma}^{arrays} \cdot dt$ represents the shear strain on the primary slip. Here, the dislocation arrays as the primary slip installed in grain A are $(\bar{1}11)[101]$. In grain A, all slips of $\{111\} < 01\bar{1} >$ except $(\bar{1}11)[101]$ contribute to relax the misfit. On the other hand, all slip systems of $\{111\} < 01\bar{1} >$ are operative in grain B.

While many combinations satisfy the conditions of Eq. (6), one optimal combination can be chosen using the principle of minimum work according to the following equations:

$$\dot{W} = \sum_{k} \tau \dot{\gamma}^{(k)} \text{ and} \quad \text{..... (10)}$$

$$M = \frac{\sum_{k} \dot{\gamma}^{(k)}}{\dot{\gamma}^{arrays}}, \quad \text{.....(11)}$$

where $\dot{W}$ is the plastic work rate and M is the normalized sum of the slip rates in all active slip systems by $\dot{\gamma}^{arrays}$. M is available to predict the secondary plastic anisotropy, as the influence of the slip length on the magnitude of stress concentration is discounted to evaluate the relationship between the grain interaction and grain orientations. In other words, the magnitude of M correlates with the difficulty of the accommodation deformation.[28] It is assumed that the critical resolved shear stresses (CRSSs), τ, for the slip systems are of the same magnitude. Minimizing $\dot{W}$ is equivalent to minimizing $\sum_{k} \dot{\gamma}^{(k)}$ under the conditions of Eq. (6).

The active slip systems and their slip rates were then evaluated when the dislocation arrays developed in grain A. The plastic work rate of $(\bar{1}11)[101]$, $\dot{W}^{arrays}$, is defined as

$$\dot{W}^{arrays} = \tau \dot{\gamma}^{arrays}, \quad \text{..... (12)}$$

where τ is the critical resolved shear stress of $\{111\} < 01\bar{1} >$. When the secondary slip system in grain A operates to accommodate the displacement incompatibility, its plastic work rate is defined as

$$\dot{W}^{acc(A)} = \tau \sum \dot{\gamma} = \tau M \dot{\gamma}^{arrays} \quad \text{..... (13)}$$

When the dislocations accumulated in grain A can transmit into grain B, the plastic work rate, $\dot{W}^{acc(B)}$, in grain B also accommodates the displacement incompatibility as defined by

$$\dot{W}^{acc(B)} = \tau \sum \dot{\gamma} = \tau M \dot{\gamma}^{arrays} \quad \text{..... (14)}$$

Here, the CRSS of $\{111\} < 01\bar{1} >$ in grain B is the same as that in grain A.

2.3. Descriptions of Orientation

The Bunge-Euler angles, φ_1, Φ, and φ_2, in the (001) pole figures of a cubic crystal transform the reference directions, x_1, x_2, and x_3 in the orthogonal grain coordinate system, onto the crystal coordinate system as shown in **Fig. 4**(a). The coordinate transformation tensor is expressed as

$$\begin{aligned}\mathbf{a} &= \mathbf{Q} \cdot \mathbf{a}' \\ &= \begin{pmatrix} \cos\varphi_1\cos\varphi_2 - \sin\varphi_1\cos\Phi\sin\varphi_2 & -\cos\varphi_1\sin\varphi_2 - \sin\varphi_1\cos\Phi\cos\varphi_2 & \sin\varphi_1\sin\Phi \\ \sin\varphi_1\cos\varphi_2 + \cos\varphi_1\cos\Phi\sin\varphi_2 & -\sin\varphi_1\sin\varphi_2 + \cos\varphi_1\cos\Phi\cos\varphi_2 & -\cos\varphi_1\sin\Phi \\ \sin\Phi\sin\varphi_2 & \sin\Phi\cos\varphi_2 & \cos\Phi \end{pmatrix} \begin{pmatrix} a_1' \\ a_2' \\ a_3' \end{pmatrix}\end{aligned} \quad \text{..... (15)}$$

where **Q** is the coordinate transformation tensor, **a** is the vector in the orthogonal grain coordinate system, and **a'** is

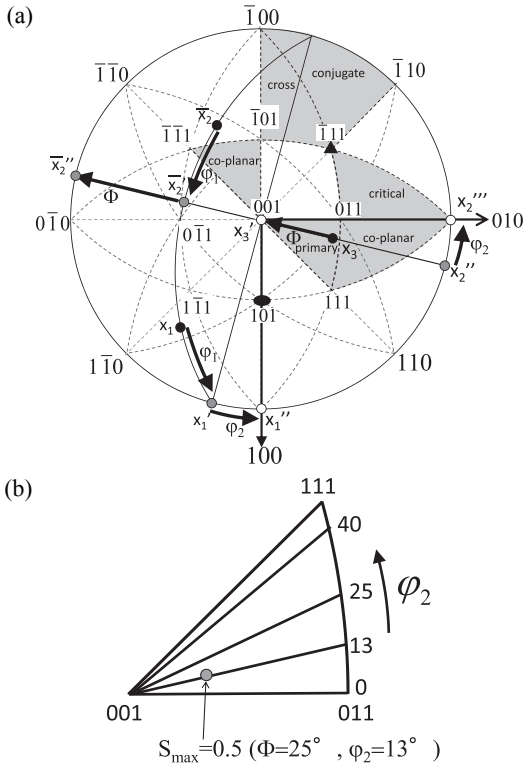

Fig. 4. Definition of Euler angles, φ_1, Φ, and φ_2: (a) The orthogonal grain coordinate system (x_1, x_2, x_3) and the crystal coordinate system (h, k, l), and (b) the range of φ_2 on the normal stereo triangle [001]-[011]-[111]. S_{max} is the maximum Schmid factor in grain A.

the vector in the crystal coordinate system. Because the primary slip system $(\bar{1}11)[101]$ preferentially operates in grain A, the maximum Schmid factor, S_{max}, of 0.5 is given at Φ = 25° and φ_2 = 13° in grain A, as shown in Fig. 4(b). The deformation behavior in grain A is represented by sections φ_2 = 0, 13, 25, and 40° (φ_1 = 0–180°, Φ = 0–G°, φ_2 = 0–45°: G depends on the value of φ_2). The accommodation deformation in grain B was also evaluated within a range of φ_1 = 0–90°, Φ = 0–90°, and φ_2 = 0–90°. Although the grain boundary orientation is not accounted for in this model, the solutions for Eqs. (7) and (8) all involve the grain boundary orientations for grain A. M_{min} and M_{max} are represented by the minimum and maximum M in each φ_2 cross section, respectively.

3. Results and Discussion

3.1. Influence of Orientation on Active Slip Systems and their Slip Rates in a Soft Grain

Figure 5 shows the contour of M in sections φ_2 = 0, 13, 25, and 40° when the displacement incompatibility at the grain boundary due to $(\bar{1}11)[101]$ dislocation arrays induces plastic deformation in grain A. M ranges from 0.00 to 2.00. The orientations of both M_{min} and M_{max} are represented by the lines in all φ_2 cross sections shown in Fig. 5. In section φ_2 = 0°, M_{min} is from φ_1 = 90° and Φ = 0° to φ_1 = 125° and Φ = 45°, and M_{max} is from φ_1 = 27° and Φ = 0° to φ_1 = 25° and Φ = 45° (Fig. 5(a)). In section φ_2 = 13°, M_{min} is from φ_1 = 77° and Φ = 0° to φ_1 = 120° and Φ = 46°, and M_{max} is from φ_1 = 14° and Φ = 0° to φ_1 = 13° and Φ = 46° (Fig. 5(b)). In section φ_2 = 25°, M_{min} is from φ_1 = 65° and Φ = 0° to φ_1 = 117° and Φ = 48°, and M_{max} is from φ_1 = 2° and Φ = 0° to φ_1 = 2° and Φ = 48° (Fig. 5(c)). In section φ_2 = 40°, M_{min} is from φ_1 = 50° and Φ = 0° to φ_1 = 112° and Φ = 52°, and M_{max} is from φ_1 = 167° and Φ = 0° to φ_1 = 168° and Φ = 22° (Fig. 5(d)). In section φ_2 = 40°, M_{max} exists within the range of Φ of 0–22°, as shown in Fig. 5(d), resulting in the appearance of a peak in the contour. The closer the orientation is to M_{max}, the steeper the contour interval of M. The area of M < 1 is much larger than that of $M \geq 1$ in all sections. Here, the sections are divided into regions 1, 2, and 3, as shown in Fig. 5, in which specific sets of slip systems are active. In sections φ_2 = 0–35°, only one slip system, *i.e.*, $(\bar{1}11)[\bar{1}\,\bar{1}0]$ or $(\bar{1}11)[01\bar{1}]$, can accommodate the

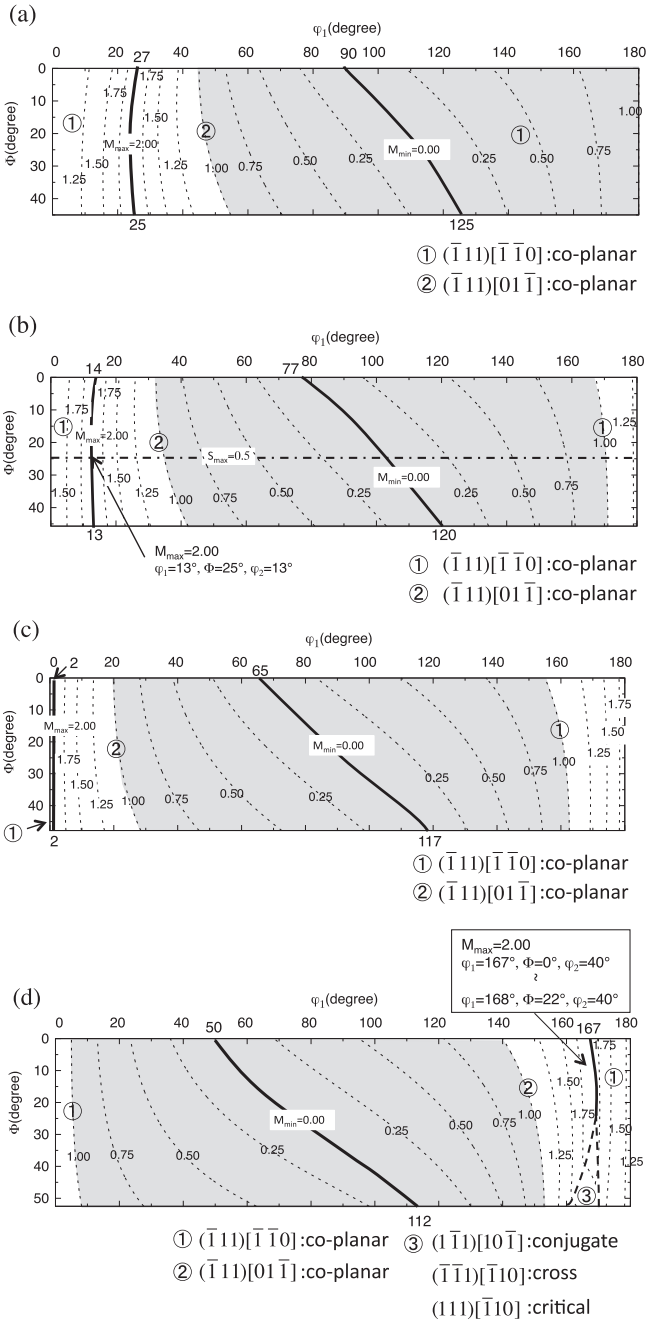

Fig. 5. Dependence of M and active slip systems on the tensile axis in grain A with respect to orientation: (a) φ_2 = 0°, (b) φ_2 = 13°, (c) φ_2 = 25°, and (d) φ_2 = 40°. The bold lines and bold dashed lines represent the boundaries of regions 1, 2, and 3, which indicate a set of active slip systems.

displacement incompatibility at the grain boundary, as shown in Figs. 5(a)–5(c). The boundaries of the two regions correspond to the lines of either M_{max} or M_{min}. In sections $\varphi_2 =$ 40–45°, the line for M_{min} also shows the boundary of regions 1 and 2 (Fig. 5(d)). Almost all orientations exhibited only one operational slip system that accommodates the displacement incompatibility. However, near the orientation of M_{max}, three slip systems, $(1\bar{1}1)[10\bar{1}]$, $(\bar{1}\,\bar{1}1)[\bar{1}10]$, and $(111)[\bar{1}10]$, are active in region 3, as shown in Fig. 5(d), which results in lower M values than M_{max} (2.00).

The representative slip propagations from dislocation movements near the grain boundaries are dislocation reflection, dislocation absorption, and dislocation emission.[27] Reflection dislocation involves the movement of dislocations back into the soft grain. The movement of reflected dislocations also accommodates the displacement incompatibility due to interactions between the dislocations and grain boundary. In this section, the plastic work rate of the accommodation deformation in grain A, $\dot{W}^{acc(A)}$, is compared with that of the arrays, $\dot{W}^{arrays}$. The orientations are classified into the following two groups by Eqs. (12) and (13) as M varies from 0.00 to 2.00, as shown in Fig. 5: (1) orientations given by $\dot{W}^{acc(A)} < \tau\dot{\gamma}^{arrays}$ ($M < 1$), and (2) orientations given by $\dot{W}^{acc(A)} \geq \tau\dot{\gamma}^{arrays}$ ($M \geq 1$). Under the first condition, *i.e.*, $\dot{W}^{acc(A)} < \tau\dot{\gamma}^{arrays}$ ($M < 1$), one operating secondary slip system can compensate for the plastic work rate of the arrays and fully accommodate the displacement incompatibility; the displacement incompatibility in the orientation of $\dot{W}^{acc(A)} < \tau\dot{\gamma}^{arrays}$ is only slightly important to the stress concentration. Under the second condition, *i.e.*, $\dot{W}^{acc(A)} \geq \tau\dot{\gamma}^{arrays}$ ($M \geq 1$), a secondary slip deformation cannot completely accommodate the displacement incompatibility because $\dot{W}^{acc(A)}$ is higher than $\dot{W}^{arrays}$. Even in the orientation $\dot{W}^{acc(A)} \geq \tau\dot{\gamma}^{arrays}$, only one slip system is active, except in region 3, and both slip systems in regions 1 and 2 are co-planar. Thus, a displacement incompatibility may exist in the soft grain.

3.2. Restrictions of Secondary Slip in the Soft Grain

In cyclically deformed nitrogen-strengthened austenitic steel, accommodation deformation in the soft grain has not been detected.[11] Dislocation accumulation occurring as a result of the applied stress being less than the macroscopic yield is constrained in balance with the back stress under cyclic deformation. *In situ* observation during tension mode enables a study of the dislocation and grain boundary interactions for 304 stainless steel, where a dislocation accumulation and dislocation emission were observed.[27] The reflection process was only detected at the very beginning of the interaction. Furthermore, a dislocation reflection occurred on a different slip plane than the primary one. A dislocation reflection on the primary slip plane is difficult to adopt for accommodation deformation after the accumulated dislocation structure develops. Therefore, it is necessary to consider the restriction of the slip plane for accommodation deformation.

When the secondary slip, *i.e.*, $\{111\} < 01\bar{1} >$, is restricted to its slip plane without $(\bar{1}11)$, accommodation deformation can be seen in sections $\varphi_2 =$ 0, 5, and 10–45°, as shown in **Fig. 6**. The restriction of slip plane $(\bar{1}11)$ resulted in an increased M value in all orientations except M_{min}. Thus, the

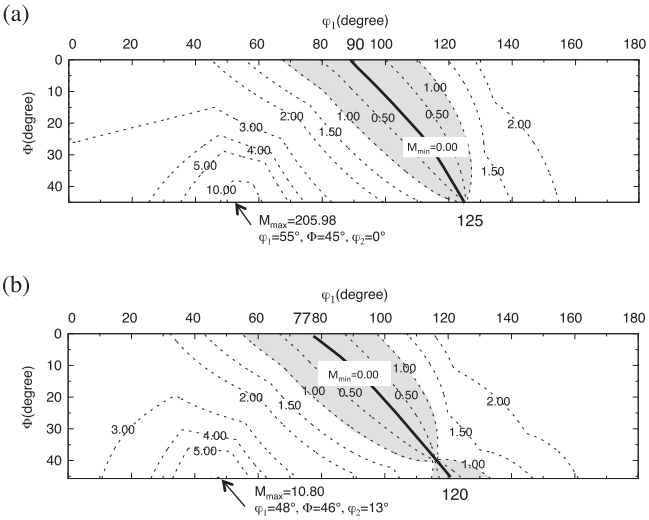

Fig. 6. Dependence of M on the orientation in sections (a) $\varphi_2 = 0°$ and (b) $\varphi_2 = 13°$, when the secondary slip on the primary slip plane (dislocation reflection) is suppressed.

orientation area of $M \geq 1$ expands, and M_{max} becomes much higher than 2.00. The highest M_{max} value in all sections is 205.98, which occurred in section $\varphi_2 = 0°$. In addition, the active slip systems did not depend on the M value in all orientations. The grain boundary plane in the orientation of M_{max} in section $\varphi_2 = 0°$ is perpendicular to $(1\bar{1}1)$, *i.e.*, the $\sum 3$ boundary. Accommodation deformation in the soft grain can barely occur near the $\sum 3$ boundary under restricted conditions. In contrast, the orientations of M_{min} were the same in all sections regardless of the restriction of the slip systems. This result indicates that the displacement incompatibility in the orientation of $M < 1$ is negligible to the stress concentration. Therefore, a restricted secondary slip without $(\bar{1}11)$ results in a hard accommodation of the displacement incompatibility in the soft grain, and the displacement incompatibility must be accommodated in the adjacent grain.

3.3. Influence of Orientation on Active Slip Systems and their Slip Rates in the Hard Grain

When a displacement incompatibility develops at the grain boundary, the induction of plastic deformation in the adjacent (hard) grain, B, should also be taken into account. Although $\dot{\gamma}^{arrays}$ is assumed to be constant, its value depends on the orientation in grain A. The Schmid factor, S, is included to account for the activity of the primary system in the soft grain. The dash-dot line in Fig. 5(b) represents the highest Schmid factor ($S_{max} = 0.5$, $\Phi = 25°$, and $\varphi_2 = 13°$) in grain A. The orientations of S_{max} continuously cover M within the range of M_{min} to M_{max}. The displacement incompatibility is highest in the orientations of M_{max}. Therefore, accommodation deformation in grain B was evaluated in the orientation of M_{max} and S_{max} ($\varphi_1 = 13°$, $\Phi = 25°$, and $\varphi_2 = 13°$) in grain A.

The M value in grain B ranges from 1.00 to 2.20 (**Fig. 7**); most of the orientations have lower M values than M_{max} (2.00) in grain A. M_{max} in grain B ranges from 2.12 to 2.20, as plotted in each φ_2 section in Fig. 7. The highest M_{max} is in section $\varphi_2 = 45°$. It is possible to develop a stress concentration in orientations with higher M values. The active

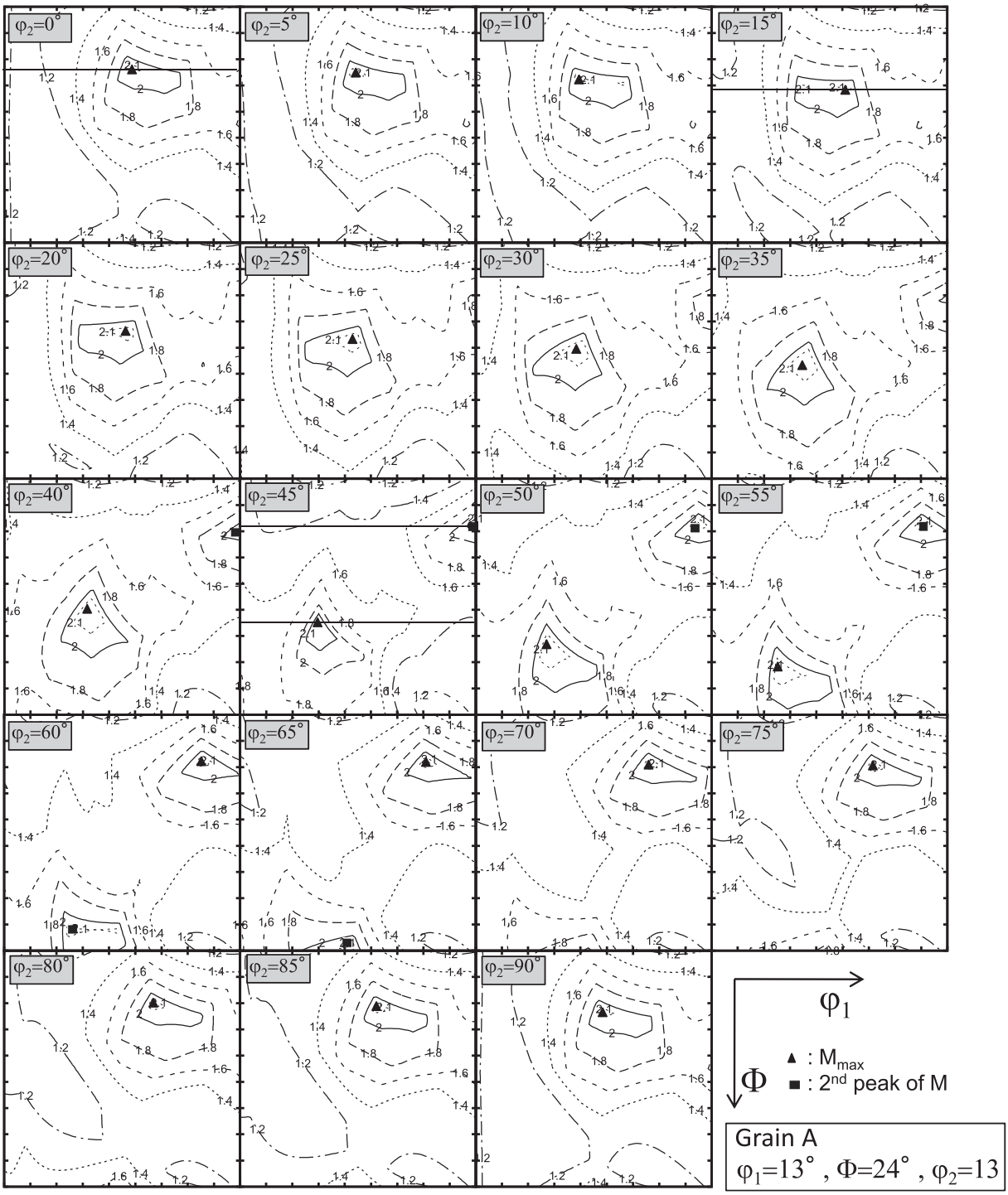

Fig. 7. Dependence of total slip rate M on the orientation in grain B. The orientation of grain A is given as $\varphi_1 = 13°$, $\Phi = 24°$, and $\varphi_2 = 13°$. The closed triangular and square plots indicate M_{max} and the second peak of M in each φ_2 section, respectively.

slip systems and their activity toward accommodation deformation in grain B were evaluated in the φ_2 sections. In each φ_2 section, Φ was fixed as the angle given in M_{max}, and the slip rates of the dominant slip systems were evaluated against φ_1, as shown in **Fig. 8**. The primary slip system was defined as the system with the highest slip rate, $\dot{\gamma}$. Accordingly, the secondary and tertiary slip systems had the second- and third-highest slip rates, respectively.

In the orientation around M_{max}, the slip rate of the primary slip system was much higher than the slip rates of the secondary and tertiary slip systems. The primary slip system is dominant for accommodation deformation in orientations around M_{max}. For example, in sections $\Phi = 23°$ and $\varphi_2 = 0°$, and $\Phi = 55°$ and $\varphi_2 = 45°$, the slip rate of the primary slip system in the orientation around M_{max} continuously increases to 1.5 and 1.75, respectively (Fig. 8). However, the slip rates of the primary slip system discontinuously drop below 1 in the orientations of M_{max}. In contrast, the slip rates of both the secondary and tertiary slip systems suddenly increase to over 0.5. As a result, there is no significant difference in the slip rates among the three slip systems around M_{max}. Thus, all three slip systems should actively accommo-

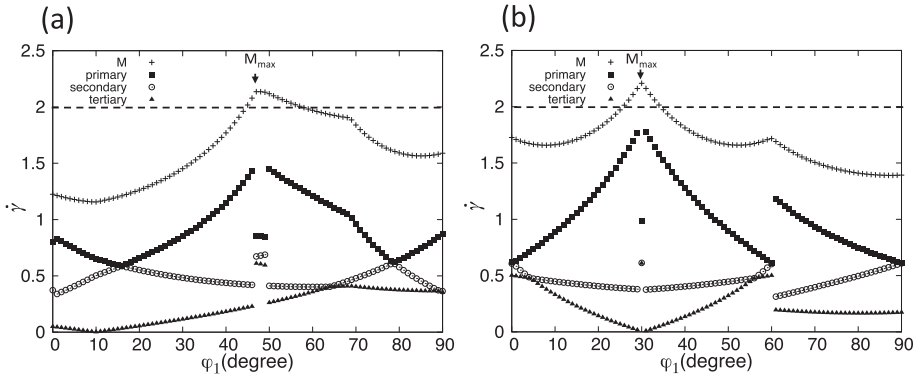

Fig. 8. Dependence of total slip rate M of the operating slip systems and the slip rate $\dot{\gamma}$ of each operating slip system on φ_1 in sections (a) $\Phi = 23°$ and $\varphi_2 = 0°$, and (b) $\Phi = 55°$ and $\varphi_2 = 45°$.

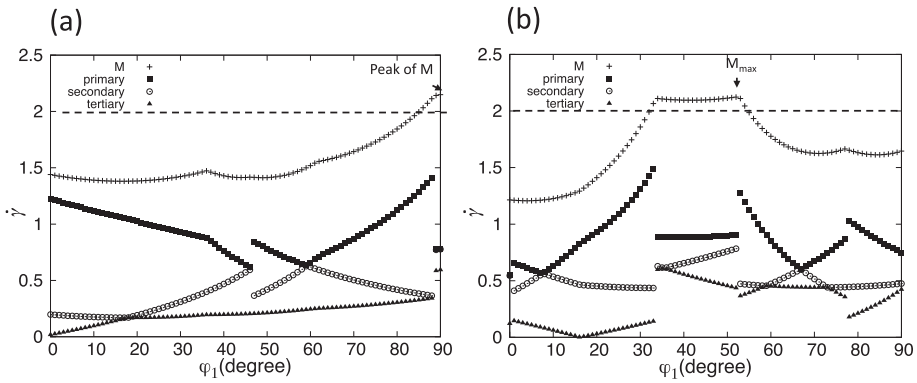

Fig. 9. Dependence of total slip rate M of the operating slip systems and the slip rate $\dot{\gamma}$ of each operating slip system on φ_1 in sections (a) $\Phi = 13°$ and $\varphi_2 = 45°$, and (b) $\Phi = 31°$ and $\varphi_2 = 15°$.

date the displacement incompatibility in the orientation around M_{max}, at which the discontinuity of the slip rates appears. A similar discontinuity of slip rates also appeared in the orientations of the second peak of M in the $\varphi_2 = 40$–$65°$ sections. In section $\Phi = 17°$ and $\varphi_2 = 45°$, a discontinuity appears in the orientation of the second peak where M is higher than 2.00 (**Fig. 9**(a)). This suggests that the primary slip system has difficulty accommodating the displacement incompatibility in this orientation. In section $\Phi = 31°$ and $\varphi_2 = 15°$, the φ_1 range of M_{max} expands from 34 to 52° (Fig. 9(b)). Thus, a displacement incompatibility occurs in orientations showing peaks of M greater than 2.00, where the slip rates of the three slip systems are similar regardless of the orientation. While the operation of the primary slip system alone cannot sufficiently satisfy the accommodation deformation in orientations of $M > 2.00$, the three slip systems operate in the orientations of these peaks. In orientations of which the slip rate of the secondary slip system is more than 0.5, the slip rates of the primary slip system are lower. For example, the slip rate of the secondary slip system is the same as that of the primary slip system in the orientations of $\varphi_1 = 17°$ and 78° in the $\Phi = 23°$ and $\varphi_2 = 0°$ section (Fig. 8(a)). Thus, the secondary slip system in grain B is responsible for the accommodation deformation. However, the tertiary slip system is rarely active in any of the orientations except for M_{max} as the slip rate of the tertiary slip system is still very low even when the slip rate of the primary slip is lowered. In orientations of $M < 2.00$, either the primary slip system or the primary and secondary slip systems are dominant for accommodation deformation. In orientations of $M > 2.00$, three slip systems must be active for accommodation deformation.

3.4. Accommodation Deformation in the Hard Grain

Accommodation deformation in the soft grain did not readily occur and was not effective for accommodating the displacement incompatibility; therefore, slip propagation into the adjacent hard grain was introduced. This involves the ejection of dislocations in the soft grain into the adjacent hard grain through the grain boundary. There are several mechanisms for a dislocation emission across grain boundaries. Dislocations can completely transmit into the adjacent grain when a direct transfer occurs.[11] However, a direct transfer is a limited case, and even a $\sum 3$ boundary can act as a significant barrier to the gliding of accumulated dislocations. The $\sum 3$ boundary also provides a site for dislocation absorption of the accumulations. In a previous study,[13] absorbed dislocations were found to be emitted through the grain boundary into the adjacent grain. Even if dislocation absorption occurs, the displacement incompatibility is eventually accommodated by the dislocation emission. In the present study, neither direct transfer nor dislocation absorption is taken into account.

The value of $\dot{W}^{acc(B)}$ is higher than $\dot{W}^{arrays}$ in all orientations since M in grain B ranges from 1.00 to 2.20. The displacement incompatibility cannot be fully accommodated by deformation in grain B because of its insufficient plastic work rate. Accordingly, the displacement incompatibility

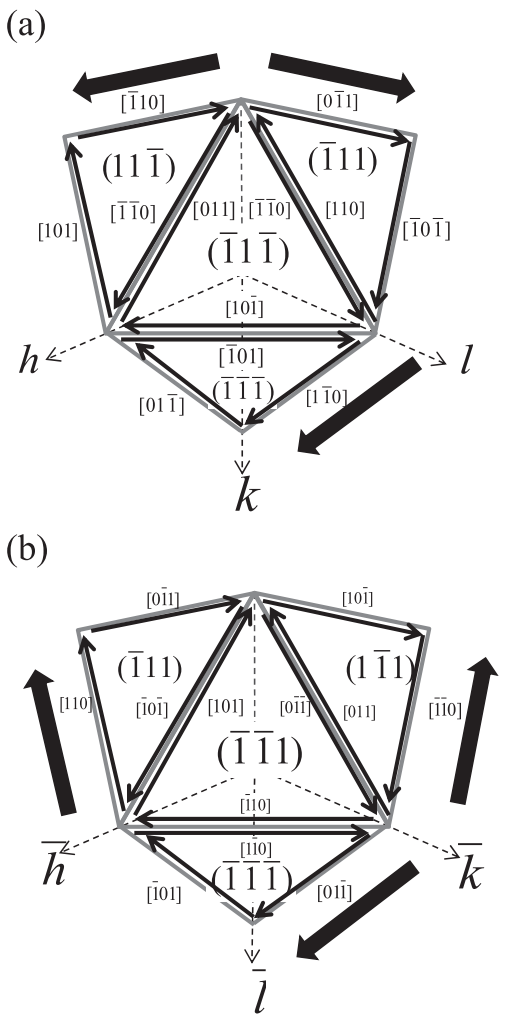

Fig. 10. Geometrical illustration of active slip systems in grain B that act to accommodate the displacement incompatibility at the orientations of (a) M_{max} in sections $\varphi_2 = 0°$ and 45° (Fig. 8), and (b) the peak of M in section $\varphi_2 = 45°$ (Fig. 9(a)).

increases with a bigger difference between $\dot{W}^{acc(B)}$ and $\dot{W}^{arrays}$. There is also a high possibility of intergranular cracking in the orientation of M_{max}. Because the slip rates of the three slip systems are almost equivalent in this orientation, the three slip systems must operate to accommodate the greatest amount of displacement incompatibility. **Figure 10** shows the active slip systems in the orientation of M_{max} or at the peak of M in sections $\varphi_2 = 0°$ and 45°. In these two sections, the active slip systems are $(\bar{1}\bar{1}\bar{1})[1\bar{1}0]$, $(11\bar{1})[1\bar{1}0]$, and $(\bar{1}11)[0\bar{1}1]$ in the orientation of M_{max} (Fig. 10(a)). At the peak of M in section $\varphi_2 = 45°$, the active slip systems are $(\bar{1}11)[110]$, $(1\bar{1}1)[110]$, and $(\bar{1}\bar{1}\bar{1})[01\bar{1}]$ (Fig. 10(b)). In all cases, the three active slip systems are on different octahedral planes. This is in agreement with the formation of crystallographic pits and protrusions on the intergranular facets.

3.5. Intergranular Cracking Due to Grain Interaction under Cyclic Deformation

Some fatigue crack nucleation models such as Stroh's cleavage model,[15] Cottrell's cleavage model,[29] and the slip-off model[16–18] have been proposed to elucidate the mechanism of microstructural cracking. Stroh's model is based on the stress levels at the head of the accumulated dislocations, which might be sufficient to cause a cleavage fracture; the dislocations can squeeze together with enough strength to produce a crack nucleus. The slip-off model assumes that a separation occurs along an active slip plane with highly dense dislocations. These models consider only one slip system and provide facets through transgranular cracking. Cottrell's cleavage model[29] also provides a method for showing a transgranular fracture. In this method, the dislocations of two slip systems interact to form a sessile dislocation with a Burgers vector normal to the cleavage plane {001}. However, no cracking on {001} has been reported.

Bache[30] proposed an advanced Stroh's model, which extended Stroh's model to include one grain (source) and its adjacent grain (failure). Essentially, the dislocation arrays in the soft grain induce dislocations on a slip plane in the adjacent grain. The soft grain, which is favorably orientated for a slip, generates a dislocation accumulation at the boundary with the adjacent hard grain. This accumulation generates the required combination of shear and tensile stresses on the unfavorably orientated cracking plane, which induces facet formation in combination with the applied principal stress. The model may be applied to intergranular cracking in addition to transgranular cracking if it accounts for grain boundary sliding.

The models mentioned above cannot elucidate intergranular cracking. The mismatching of slip traces on the matching facets opposite the fracture surfaces[11] suggests the presence of a secondary slip deformation due to a displacement incompatibility at the grain boundary. In the present study, we propose an intergranular cracking process due to such displacement incompatibility near the grain boundary. Firstly, dislocation arrays develop in the soft grain. Then, displacement incompatibility occurs at the grain boundary. In the adjacent grain, three slip systems operate to accommodate the displacement incompatibility. However, slip deformation cannot fully accommodate the displacement incompatibility because it is insufficient for the necessary plastic work. When the stress concentration due to a displacement incompatibility is highest at the grain boundary, three active slip systems are required to operate in the adjacent grain. The three slip systems are considered as GNDs in the many transpositions that were formed and were observed in the local strain gradient. The dislocation density increases near the grain boundary in the adjacent grain. Because a secondary slip deformation cannot completely accommodate the displacement incompatibility, the stress concentration due to a displacement incompatibility such as an opening displacement at the grain boundary continues to accumulate. The deformation directions of the three slip systems geometrically surround the normal to {111} in orientations of M_{max} and at the peak of M (Fig. 10). This suggests that the stress field exists near the normal to {111}. The combination of stress concentration sufficient to open the grain boundary and the assembly of dislocations on the three slip systems at the grain boundary may be the cause of intergranular cracking.

4. Conclusions

An accommodation deformation model based on the

Taylor theory was applied to intergranular cracking due to displacement incompatibility at a grain boundary during high-cyclic fatigue of face-centered cubic polycrystalline materials. Dislocation arrays were installed in the soft (yield) grain, and secondary slips to accommodate the displacement incompatibility in the soft grain or adjacent hard (non-yielded) grain were discussed as follows:

(1) If a secondary slip in the soft grain is active on the same plane as the dislocation arrays, it accommodates the displacement incompatibility in almost all orientations. However, dislocation reflection on the primary slip plane is difficult to adopt for accommodation deformation. When the secondary slip in the soft grain is restricted to a plane without a primary slip plane, accommodation deformation in the soft grain can barely occur.

(2) To accommodate the displacement incompatibility, slip systems in the adjacent grain are required to operate in almost all orientations. Around the orientations given the highest slip rates (M_{max}) in each φ_2 cross section, three slip systems are operational when the displacement incompatibility is highly accumulated. Thus, the three slip systems should operate on different octahedral slip planes. However, the displacement incompatibility is not completely accommodated, and a stress field exists near the normal to {111}. The combination of sufficient stress concentration to open the grain boundary and the assembly of dislocations on the three slip systems at the grain boundary may cause intergranular cracking.

Acknowledgement

The authors thank Prof. K. Sekine, Yokohama National University, for his valuable discussion. This study was supported by a Grant-in-Aid for JSPS Fellows from the Japan Society for the Promotion of Science.

REFERENCES

1) D. Eylon and J. Strope: *J. Mater. Sci.*, **14** (1979), 345.
2) D. Eylon: *J. Mater. Sci.*, **14** (1979), 1914.
3) D. L. Davidson and D. Eylon: *Metall. Mater. Trans. A*, **11A** (1980), 837.
4) O. Umezawa, K. Nagai and K. Ishikawa: *Tetsu-to-Hagané*, **76** (1990), 924 (in Japanese).
5) H. Yokoyama, O. Umezawa, K. Nagai, T. Suzuki and K. Kokubo: *Metall. Mater. Trans. A*, **31A** (2000), 2793.
6) M. R. Bache, W. J. Evans and H. M. Davies: *J. Mater. Sci.*, **32** (1997), 3435.
7) A. L. Pilchak, A. Bhattacharjee, A. H. Rosenberger and J. C. Williams: *Int. J. Fatigue*, **31** (2009), 984.
8) C. J. Szczepanski, S. K. Jha, J. M. Larsen and J. W. Jones: *Metall. Mater. Trans. A*, **39A** (2008), 2841.
9) I. Bantounas, D. Dye and T. C. Lindley: *Acta Mater.*, **57** (2009), 3584.
10) E. E. Sackett, L. Germain and M. R. Bache: *Int. J. Fatigue*, **29** (2007), 2015.
11) O. Umezawa and K. Nagai: *Metall. Mater. Trans. A*, **29A** (1998), 809.
12) O. Umezawa and K. Nagai: *ISIJ Int.*, **12** (1997), 1170.
13) O. Umezawa: *ISIJ Int.*, **10** (2009), 1624.
14) Q. Dai, Z. Yuan, X. Chen and K. Chen: *Mater. Sci. Eng. A*, **517** (2009), 257.
15) A. N. Stroh: *Adv. Phys.*, **6** (1957), 418.
16) Y. Tomota and S. Endo: *ISIJ Int.*, **30** (1990), 656.
17) Y. Tomota and Y. Xia: *Acta Mater.*, **46** (1998), 1577.
18) O. Ojima, Y. Adachi, Y. Tomota, K. Ikeda and Y. Katada: *J. Jpn. Inst. Met.*, **73** (2009), 283 (in Japanese).
19) G. I. J. Taylor: *Inst. Met.*, **62** (1938), 307.
20) P. V. Houtte, S. Li, M. Seefeldt and L. Delannay: *Int. J. Plasticity*, **21** (2005), 589.
21) G. Sachs: *Z. Ven. Dt. Ing.*, **72** (1928), 734.
22) F. Roter, P. Eisenlohr, T. R. Biele and D. Raabe: Crystal Plasticity Finite Element Methods in Material Science and Engineering, WILEY-VCH Verlag GmbH & Co. KGaA, Weinheim, (2010), 100.
23) K. Sekine and J. Wang: Proc. Plast.'95, Gordon & Breach Science Publishers, New York, (1995), 313.
24) M. Crumbach, M. Goerdeler and G. Gottstein: *Acta. Mater.*, **54** (2006), 3275.
25) D. D. Tjahjanto, P. Eisenlohr and F. Roters: Proc. 12th Int. ESAFORM Conf. on Material Forming, ESAFORM, Enschede, (2009).
26) P. Eisenlohr, D. D. Tjahjanto, T. Hochrainer, F. Roter and D. Raabe: *Int. J. Mater. Res.*, **100** (2009), 500.
27) Z. Shen, R. H. Wagoner and W. A. T. Clark: *Acta Metall.*, **36** (1988), 3231.
28) M. Morita and O. Umezawa: *Mater. Trans.*, **52** (2011), 1595.
29) A. H. Cottrell: *Trans. Am. Inst. Min. Engrs.*, **212** (1958), 192.
30) M. R. Bache: *Int. J. Fatigue*, **25** (2003), 1079.